

Metabolism of the lipophilic phycotoxin 13-Desmethylspirolide C using human and rat in vitro liver models

Jimmy H Alarcan, Estelle Dubreil-Cheneau, Antoine H Huguet, Romulo Araoz, Françoise Brée, Ludovic Le Hégarat, Belkacem Bouaita, Dominique Hurtaud-Pessel, Albert Braeuning, Stefanie Hessel-Pras, et al.

▶ **To cite this version:**

Jimmy H Alarcan, Estelle Dubreil-Cheneau, Antoine H Huguet, Romulo Araoz, Françoise Brée, et al.. Metabolism of the lipophilic phycotoxin 13-Desmethylspirolide C using human and rat in vitro liver models. Toxicology Letters, 2019, 307, pp.17-25. 10.1016/j.toxlet.2019.02.012 . anses-02083152

HAL Id: anses-02083152

https://anses.hal.science/anses-02083152

Submitted on 22 Oct 2021

HAL is a multi-disciplinary open access archive for the deposit and dissemination of scientific research documents, whether they are published or not. The documents may come from teaching and research institutions in France or abroad, or from public or private research centers.

L'archive ouverte pluridisciplinaire **HAL**, est destinée au dépôt et à la diffusion de documents scientifiques de niveau recherche, publiés ou non, émanant des établissements d'enseignement et de recherche français ou étrangers, des laboratoires publics ou privés.



Distributed under a Creative Commons Attribution - NonCommercial 4.0 International License

Version of Record: https://www.sciencedirect.com/science/article/pii/S0378427419300499
Manuscript_dd3d9ec80b8527601499a4c09da6c94a

Metabolism of the lipophilic phycotoxin 13-desmethylspirolide C using human and rat *in vitro* liver models

Jimmy Alarcan[a,b], Estelle Dubreil[c], Antoine Huguet[a], Romulo Aráoz[d,e], Françoise Brée[f], Belkacem Bouaita[g], Dominique Hurtaud-Pessel[c], Albert Braeuning[b] , Stefanie Hessel-Pras[b], Alfonso Lampen[b], Ludovic Le Hégarat[a,*] and Valérie Fessard[a]

[a]Toxicology of Contaminants Unit, French Agency for Food, Environmental and Occupational Health & Safety, ANSES, Fougères 35306, France; jimmy.alarcan@anses.fr, antoine.huguet@anses.fr, ludovic.lehegarat@anses.fr, valerie.fessard@anses.fr

[b]BfR, German Federal Institute for Risk Assessment, Department of Food Safety, Max Dohrn Strasse 8-10, 10589 Berlin, Germany; Jimmy.Alarcan@bfr.bund.de, Albert.Braeuning@bfr.bund.de, Stefanie.Hessel-Pras@bfr.bund.de, Alfonso.Lampen@bfr.bund.de

[c]Analysis of Residues and Contaminants Unit, French Agency for Food, Environmental and Occupational Health & Safety, ANSES, Fougères 35306, France; estelle.dubreil@anses.fr, dominique.pessel@anses.fr

[d]CNRS, Institut de Neurosciences (Neuro-PSI), UMR9197, 91191 Gif sur Yvette, France

[e]CEA/DRF/JOLIOT/SIMOPRO, Université Paris-Saclay, 91191 Gif sur Yvette, France; Romulo.ARAOZ@cea.fr

[f]Eurosafe, Parc d'Affaires La Bretêche, 35760 Saint Grégoire, France; francoise.bree@eurosafe.fr

[g]Biopredic International, Parc d'Affaires La Bretêche, 35760 Saint Grégoire, France; belkacem.bouaita@biopredic.com

© 2019 published by Elsevier. This manuscript is made available under the CC BY NC user license
https://creativecommons.org/licenses/by-nc/4.0/

Corresponding author:

Ludovic Le Hégarat

Adress: ANSES, French Agency for Food, Environmental and Occupational Health & Safety, Fougères Laboratory, Toxicology of contaminants Unit, 10B rue Claude Bourgelat, 35306 Fougères, France

Phone: +33-(0)-299-172747.

Fax: +33-(0)-299-947880.

E-mail: ludovic.lehegarat@anses.fr

Abbreviations[1]: α-BgTx: alpha-bungarotoxin; Cl_{int}: intrinsic clearance; CYP: cytochrome P450; EFSA: European Food Safety Authority; *fm*: fraction metabolized; HLM: human liver microsome; ip: intra-peritoneal; LC/HRMS: liquid chromatography/high resolution mass spectrometry; LOD: limit of detection; LOQ: limit of quantification; nAChR: nicotinic acetylcholine receptor; qPCR: quantitative polymerase chain reaction; 13-SPX-C: 13-desmethylspirolide C

[1]**Abbreviations:** α-BgTx: alpha-bungarotoxin; Cl_{int}: intrinsic clearance; CYP: cytochrome P450; EFSA: European Food Safety Authority; *fm*: fraction metabolized; HLM: human liver microsome; ip: intra-peritoneal; LC/HRMS: liquid chromatography/high resolution mass spectrometry; LOD: limit of detection; LOQ: limit of quantification; nAChR: nicotinic acetylcholine receptor; qPCR: quantitative polymerase chain reaction; 13-SPX-C: 13-desmethylspirolide C

Abstract

13-desmethylspirolide C (13-SPX-C) is a phycotoxin produced by dinoflagellates which can accumulate in shellfish. 13-SPX-C induces neurotoxic effects in rodents through blockade of nicotinic acetylcholine receptors. As no human intoxication has been to date attributed to the consumption of 13-SPX-C-contaminated seafood, this toxin is not regulated according to the Codex Alimentarius. Nevertheless, shellfish consumers can be exposed to 13-SPX-C via shellfish consumption. In order to follow the fate of the toxin after ingestion and to verify whether metabolic detoxification could explain the lack of human intoxications, we assessed the metabolism of 13-SPX-C using several *in vitro* liver systems. First, both phase I and II reactions occurring with rat and human liver S9 fractions were screened. Our results indicated that 13-SPX-C was almost completely metabolized with both rat and human liver S9. Using a receptor binding assay towards nicotinic acetylcholine receptors we demonstrated that the resulting metabolites showed less affinity towards nicotinic acetylcholine receptors than 13-SPX-C. Finally, we showed that 13-SPX-C induced a pronounced increase of gene expression of the drug-metabolizing enzyme cytochrome P450 (CYP) CYP1A2. The role of this CYP in 13-SPX-C metabolism was clarified using an innovative *in vitro* tool, CYP1A2-Silensomes™. In summary, this study highlights that liver first-pass metabolism can contribute to the detoxification of 13-SPX-C.

Keywords: 13-desmethylspirolide C, metabolism, Silensomes™, CYP, nicotinic acetylcholine receptors

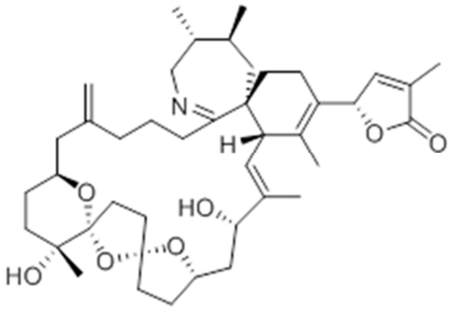
1. Introduction

13-desmethyl spirolide C (13-SPX-C) belongs to a particular group of lipophilic marine biotoxins, the cyclic imine toxins (Figure 1). It is mainly produced by dinoflagellates of the species *Alexandrium ostenfeldii* and *A. peruvianum* (Cembella et al., 2000, Touzet et al., 2008). 13-SPX-C accumulates in shellfish and is recurrently detected during monitoring (Amzil et al., 2007, Picot et al., 2013). Based on occurrence data provided by numerous countries, the EFSA (bulletin #1628) reported that 13-SPX-C is detected at a typical concentration of 20-50 µg/kg shellfish, but some authors also reported higher levels of contamination (e.g. 226 µg/kg shellfish by Miles et al., 2010). Currently, there is no regulation for 13-SPX-C in seafood worldwide including Europe due to lack of evidence between human intoxication and 13-SPX-C levels in shellfish.

Structurally, it features a unique cyclic imine moiety involved in potent antagonism towards muscle and neuronal nicotinic acetylcholine receptors (nAChRs) (Gill et al., 2003, Bourne et al., 2010, Aráoz et al., 2015). Classified as fast-acting toxin, 13-SPX-C induces rapid death, between 3 and 20 minutes, after intra-peritoneal injection or gavage to rodents by blocking respiratory muscles (Gill et al., 2003, Munday et al., 2012). Intraperitoneal and oral LD_{50} were estimated to 6.9 and 160 µg/kg body weight, respectively (Munday et al., 2012). Besides, after a single oral administration of 27.9 µg/kg to mice, no clinical effect was reported and only low amounts of 13-SPX-C were detected in blood and urine (Otero et al., 2012). Nevertheless, *in vitro* studies in a human intestinal barrier model showed that 13-SPX-C can easily cross the monolayer (Espiña et al., 2011). Taken together, these results suggest that the toxin can be absorbed along the gastrointestinal tract and reach the liver where biotransformation of 13-SPX-C occurs. Indeed, several phase I metabolites of 13-SPX-C, which are likely to be produced by cytochrome P450 (CYP) enzymes, have been described using human liver microsomes (HLM) (Hui et al., 2012).

In order to better characterize the fate of 13-SPX-C in humans due to liver metabolism, we undertook a multi-endpoint approach by i) screening main phase I and phase II reactions in rat and human liver S9 mix for 13-SPX-C metabolism, ii) investigating the receptor-binding activity of S9-generated 13-SPX-C metabolites using the *Torpedo*-nAChRs binding assay, iii) studying the transcriptional regulation of nuclear receptors and drug-metabolizing enzymes in the human HepaRG hepatic cell line, and finally iv) identifying the implication of CYP1A2 in the metabolism of 13-SPX-C using the Silensomes™ technology.

Figure 1. Chemical structure of 13-SPX-C



2. Materials and methods

2.1 Chemicals

13-SPX-C was purchased from the National Research Council Institute for Marine Biosciences (Halifax, NS Canada). Omeprazole, rifampicin, alamethicin (Trichoderma viride), D-saccharic acid 1,4-lactone monohydrate (D-saccharolactone), reduced L-glutathione (GSH), uridine 5′-diphosphoglucuronic acid triammonium salt (UDPGA), adenosine 3'-phosphate 5'-phosphosulfate lithium salt hydrate (PAPS) and S-(5′-adenosyl)-L-methionine p-toluenesulfonate salt (SAM), streptavidin-HRP and α-BgTx were purchased from Sigma-Aldrich (St. Louis, MO, USA). o-Phenylenediamine (OPD) tablets were obtained from DAKO (Glostrup, Denmark). Biotin-α-BgTx was obtained from Molecular Probes (Eugene, OR, USA). Reduced nicotinamide adenine dinucleotide phosphate (NADP+), glucose 6-phospate (G6P), magnesium chloride hexahydrate, potassium chloride, Na_2HPO_4, and NaH_2PO_4 were purchased from Carl Roth (Karlsruhe, Germany). All other chemicals including acetonitrile (ACN), methanol (MeOH) and dimethyl sulfoxide (DMSO) were of analytical grade and purchased from Fisher Scientific (Leicestershire, England). Formic acid was purchased from Merck (Darmstadt, Germany). Deionised water was prepared using a Milli-Q system (Millipore, Bedford, MA, USA). β-Naphtoflavone- and phenobarbital-induced Sprague Dawley rat (pool of 4 male animals) S9 fraction, human (pool of 3 male donors) hepatic S9 fraction, as well as Silensomes™ were purchased from Biopredic International (Rennes, France).

2.2 Cell culture

HepaRG cells were cultured as previously published (Le Hegarat et al., 2010). Briefly, HepaRG cells (passages 13–19) were seeded at 30,000 cell/cm^2 in 96-well (for High Content

Analysis) or 12-well plates (for qPCR assays) in culture medium (Williams' medium E with GlutaMAX-I, supplemented with 10% fetal bovine serum, 50 IU/ml penicillin, 50 µg/ml streptomycin, 2 mM L-glutamine, 5 µg/ml bovine insulin, and 50 µM hydrocortisone hemisuccinate). After 2 weeks, the cells were cultured in the same medium supplemented with 1.7% DMSO (differentiation medium) for two additional weeks. The medium was renewed every 2 to 3 days.

2.3 Combined phase I and II metabolism analysis of 13-SPX-C

In order to assess a broader spectrum of biotransformation process, several phase II reactions were screened along with phase I metabolism: gluruconidation, sulfation, glutathione conjugation and methylation. The procedure was conducted as followed: rat or human liver S9 fractions were first cooled on ice for 15 min in the presence of alamethicin (0.025 mg/ml). Then, D-saccharolactone (10 mM), UDPGA (6 mM), GSH (5 mM), PAPS (0.2 mM), SAM (0.1 mM), $NADP^+$ (4 mM), G6P (5 mM), KCl (33 mM), $MgCl_2$ (8 mM), and 0.1 M sodium phosphate buffer (Na_2HPO_4 + NaH_2PO_4, pH 7.4) were added. An experimental volume of 0.5 mL containing phase I and II co-factors (final concentrations as described above), S9-fraction (final protein concentration 2.2 mg/mL), and 100 nM 13-SPX-C were incubated in a water bath at 37 °C for 3 h. Reactions were stopped by adding 0.5 mL of ice-cold MeOH. After 20 min of centrifugation (14 000 × g) at 4°C, samples were analyzed or stored at -80°C until analysis. As a negative control, the same procedure was followed with heat-inactivated S9 fraction (45 min at 60°C prior to incubation with co-factors and 13-SPX-C). Two independent experiments were conducted with the same S9 batches.

2.4 Purification of *Torpedo* electrocyte membranes

Torpedo electrocyte membranes rich in nAChRs were purified from the electric organ of *Torpedo marmorata* as described previously (Hill et al., 1991, Vilariño et al., 2009).

2.5 Microplate receptor-binding assay

Prior to analysis, the samples generated after S9 incubations were evaporated at 40°C under a stream of N_2. The dried samples were resuspended in 100 µL MeOH. Dilutions of the samples (6%) were prepared in Tris-buffered saline-bovine serum albumine (TBS-BSA) (150 mM NaCl, 50 mM Tris-HCl, 0.5% BSA, pH 7.4). The binding activity of 13-SPX-C and its metabolites was assessed using the non-radioactive microplate receptor-binding assay as described by Aráoz et al. (Aráoz et al., 2012). Briefly, a 96-well microplate coated with *Torpedo*-nicotinic acetylcholine receptors was incubated overnight at 4°C with 100 µL of samples. MeOH concentration in the samples was 6%. At this concentration, MeOH does not interfere with the binding assay, as the tolerance of the method to MeOH is higher (up to 10%) (Rubio et al., 2014). The next day, the microplate was incubated at room temperature for 30 min, after which a volume of 50 µL biotin-α-bungarotoxin (BgTx) (240 nM) was added to each well prior to incubation for 30 min at room temperature under constant shaking. The wells were washed thrice with 250 µL washing buffer (TBS containing 0.1% Tween 20), and 100 µL of streptavidin-HRP (220 ng/nL protein) was added immediately afterwards to each well, followed by further incubation for 30 min. For quantifying the binding inhibition, the wells were washed thrice as described above; and 100 µL of freshly prepared peroxidase substrate OPD (as indicated by the supplier) was added to each well. After 5 min, the enzymatic reaction was stopped by adding 100 µL of 0.5 M H_2SO_4. Data were recorded using an ELISA reader (CLARIOstar, BMG LABTECH, Champigny sur Marne, France). The

optical density obtained at 492 nm (OD_{492nm}) was transformed into an inhibition percentage using the following equation:

inhibition % = 100× (100% signal - signal sample)/(100% signal - 100% inhibition)

100% of signal represents the absorption data from wells in which *Torpedo* membranes were incubated in the absence of toxins/extracts; signal sample is the absorption data of tested samples; 100% inhibition is the absorption data obtained after incubating *Torpedo*-nAChRs with 10 µM α-BgTx. Each sample was measured in two independent experiments as triplicates.

2.6 Real time quantitative Polymerase Chain Reaction (RT-qPCR) analysis

For qPCR assays, after 24 h incubation with 13-SPX-C, solvent control (0.64% MeOH) or drug metabolism-inducer positive controls (50 µM omeprazole or 10 µM rifampicin), cells were washed twice with PBS. Total RNA extraction was then performed using the Total RNA isolation NucleoSpin RNA II kit from Macherey Nagel (Hoerd, France) following the manufacturer's protocol. RNA concentration and quality was determined by spectrophotometric measurements with a BioSpec-nano device (Shimadzu Biotech, Marne la Vallée, France). RNA integrity was checked through electrophoresis using Experion (Bio-Rad, Marne la Coquette, France). RNA samples were then reverse transcribed into double-strand cDNA using the High Capacity RNA-to-cDNA kit (Applied Biosystems, Foster City, CA, USA) according to the manufacturer's instructions. The sequences of target genes were obtained from the National Center for Biotechnology Information (NCBI) GenBank sequence database (see references). Primers were designed with the NCBI primer designing tool (see references). For each gene, at least one primer was designed to span an exon-exon junction. All primers (Appendices Table A.1) were purchased from Sigma-Aldrich (Saint-Louis, MO, USA). Quantitative PCR was performed using a Light Cycler 1536 from Roche (Mannheim,

Germany). SYBR Green chemistry was used and reactions were performed in a total volume of 2 µl containing 1X Light cycler 1536 DNA Green Master, 1X Light cycler 1536 DNA Master mix (Roche), 300 nM of each primer, and 0.1 ng cDNA. Negative quantitative PCR controls of RNase-free water were included in each run for contamination assessment. The thermal cycling conditions were 94°C for 15 s, followed by 40 cycles of 15 s at 94°C and 30 s at 60°C with a slow ramp temperature (2.2°C/s). Light Cycler 1536 software (version 1.1.0.1112; Roche, Basel, Switzerland) was used for quantitative analysis. Melting curve analysis was used to check the specificity of each amplicon. Threshold Cqs were calculated from a baseline-subtracted curve fit. Calibration curves were established for each gene from a serial dilution of a reference sample (pool of cDNA samples). According to these calibration curves, mean relative amounts of mRNA of the target genes were calculated for each sample and then normalized to the reference gene *GAPDH*. Values are presented as fold change normalized to the solvent control. Three independent experiments were performed with single replicate.

2.7 Silensomes™-dependent phase I clearance

Silensomes™ are human pooled liver microsomes in which a single CYP has been chemically and irreversibly inactivated using mechanism-based inhibitors. CYP1A2-Silensomes™ and homologous control-Silensomes™ were prepared as described previously for CYP3A4-Silensomes™ (Parmentier et al., 2017). The inhibitor used for CYP1A2-Silensomes™ was furafylline. The homologous control-Silensomes™ were prepared under the same conditions, except that the inhibitor was replaced by an equivalent volume of solvent (Parmentier et al., 2017).

In order to investigate the involvement of CYP1A2 in 13-SPX-C metabolism, appropriate co-factors were added to CYP1A2-Silensomes™ fractions: NADPH (1 mM), $MgCl_2$ (5 mM),

and 0.1 M sodium phosphate buffer (Na_2HPO_4 + NaH_2PO_4, pH 7.4). An experimental volume of 0.1 mL containing phase I co-factors (final concentration as described above), Silensomes (final concentration 1 mg/mL) and 100 nM 13-SPX-C were incubated in a water bath at 37 °C for different times. The reaction was stopped by adding 0.1 mL of ice-cold ACN. After 20 min of centrifugation (14 000 × g) at 4°C, samples were analyzed or stored at -80°C until analysis. Homologous control Silensomes™ were used accordingly. The *in vitro* intrinsic clearances (Cl_{int}) were calculated as follows: Cl_{int} (µL/min/mg) = (slope x V) / P, where the slope is the elimination rate constant (min^{-1}) for exponential substrate loss, V is the incubation volume (µL) and P is the microsomal protein amount (mg) in the incubation. The fraction metabolized (fm) by CYP1A2 was calculated as follow: CYP1A2 fm = [1- (Cl_{int} CYP1A2-Silensomes™/ Cl_{int} Control-Silensomes™)] x 100. Three independent experiments were conducted with the same Silensomes™ batches.

2.8 13-SPX-C metabolite analysis by LC/HRMS

Metabolism investigation was conducted in two steps: the decrease of the parent compound was first measured using LC/HRMS method and then targeted metabolites were searched using MetWorks® 1.3 software (see Appendices Table A.2 for screened reactions). Analyses were conducted with a Thermo Fisher Accela LC (Thermo Fisher, Bremen, Germany) system hyphenated to an LTQ-Orbitrap XL mass spectrometer. LC separation was performed by an Agilent Zorbax Eclipse XDB-C18 column (Agilent Technologies, Santa Clara, CA, USA) (150×3.0 mm, 3.5 µm). Chromatographic separation was carried out using a binary eluent system consisting of 100 % water (A) and 5 % water/95 % ACN (v/v) (B), both containing 2 mM formate ammonium and 50 mM formic acid. The gradient conditions were set as follows: from 0 to 5 min ramp linearly from 98 to 2 % of mobile phase A and hold for 7 min, then ramp over 1 min to initial conditions and hold for 3 min to re-equilibrate the system. The flow

rate was set at 0.3 mL min^{-1}, the injection volume was 10 µL and the column oven was maintained at 25°C. 13-SPX-C was quantified using an external calibration curve with 13-SPX-C standards at 0, 5, 10, 25, 50, 75 and 100 ng/ml in MeOH/water 2:3 (v/v). The mass spectrometer was operated with an electrospray ionization probe in positive mode using the following source parameters: sheath gas flow rate: 40 arb; auxiliary gas flow rate: 15 arb; sweep gas flow rate: 2 arb; ion spray voltage: 3.5 kV; capillary temperature: 350°C; capillary voltage: 30 V; and tube lens: 100 V. The instrument was calibrated using the manufacturer's calibration solution consisting of three mass calibrators (i.e. caffeine, tetrapeptide MRFA and Ultramark) to reach mass accuracies in the 1–3 ppm range. The instrument was operated in full-scan mode from *m/z* 100–1,000 at a resolving power of 60,000 (full width at half maximum) allowing 13-SPX-C detection as protonated adduct ion $[M+H]^+$ (*m/z* 692.45208) as well as metabolite formation investigations using MetWorks® software (Thermo Fisher Scientific, Waltham, MA, USA). The extraction mass window was set at ± 5 ppm. 13-SPX-C recoveries were calculated as follow: $R_i = (c_i \times 100)/c_0$ where c_i is the measured concentration of the sample i and c_0 is the initial concentration. Each sample was measured twice and mean recovery was calculated.

2.9 Statistical analysis

GraphPad Prism 5 (GraphPad Software, Inc., La Jolla, CA, USA) was used for statistical analyses. Data were compared to the control group using one-way ANOVA followed by Dunnett's post hoc test. All error bars denote standard deviation (SD). Statistical significance is denoted as follows: *$p < 0.05$, **$p < 0.01$, ***$p < 0.001$.

3. Results

3.1 13-SPX-C metabolism in rat and human S9 fractions

First, a quantitative method for 13-SPX-C dosage using LC-HRMS was developed. A standard solution of 13-SPX-C was used to establish a linear calibration curve (R^2 = 0.99) between 5 and 100 ng/mL toxin. The limits of detection (LOD) and quantification (LOQ) were estimated using signal intensities of standard solutions at 5 and 10 ng/mL 13-SPX-C since there was no signal to noise ratio when extracting the molecular mass. LOD and LOQ values were 0.76 and 3.4 ng/mL, respectively. We then determined the recoveries of 100 nM 13-SPX-C following incubation with inactivated S9 fractions. We observed a mean recovery of 88 ± 24% with inactivated rat S9, while 87 ± 1% mean recovery was obtained with inactivated human S9 (Appendices Table A.3).

When 13-SPX-C was incubated during 3 h with native liver S9 fractions, we observed an almost full loss of the parental compound for rat S9 (97 ± 5%), and a full loss for human S9 (100 ± 0%) (Appendices Table A.4).

The detection of metabolites was investigated using MetWorks software. From the $[M+H]^+$ protonated parent ion (*m/z* 692.45208), screening for a wide panel of phase I and phase II reactions was performed based on mass shifts (Appendices Table A.2). With rat S9 fraction, one metabolite with *m/z* 708.44699 (M2a) was found in both experiments. The first experiment featured also a metabolite with *m/z* 724.44191 (M4) while the second experiment featured metabolites with *m/z* 706.43134 (M1) and *m/z* 726.45756 (M5) (Table 1). With human S9 fraction, three metabolites were found in both experiments: two with *m/z* 708.44699 (M2b and M2c) and one with *m/z* 722.42626 (M3) (Table 1). With both inactivated rat and human S9 fractions, only the protonated adduct of 13-SPX-C was detected (data not shown). Assignment of the sites of biotransformation was not performed in this study and therefore putative structures of the metabolites are not detailed.

Table 1. 13-SPX-C metabolites detected after incubation with rat or human S9 fractions and phase I and II co-factors. S9 fractions were incubated for 3 h with specific phase I and II co-factors and 100 nM of 13-SPX-C. Results were obtained from two independent experiments conducted with the same S9 fraction batches. Presence or absence of a metabolite is depicted as "+" or "-" and x/y indicates first and second experiment, respectively.

Entity	Formula	Increment mass	m/z_{calc}	m/z_{exp}	Error (ppm)	Predicted Biotransformation	t_R (min)	Rat S9	Human S9
13-SPX-C	$C_{42}H_{62}NO_7^+$	-	692.45208	692.45087	-1.75	-	5.80	-/+	-/-
M1	$C_{42}H_{60}NO_8^+$	+13.97926	706.43134	706.42902	-3.28	hydroxylation and desaturation or methylene to ketone	5.72	-/+	-/-
M2a	$C_{42}H_{62}NO_8^+$	+15.99491	708.44699	708.44565	-1.89	hydroxylation or epoxidation	5.46	+/+	-/-
M2b	$C_{42}H_{62}NO_8^+$	+15.99491	708.44699	708.44565	-1.89	hydroxylation or epoxidation	5.76	-/-	+/+
M2c	$C_{42}H_{62}NO_8^+$	+15.99491	708.44699	708.44565	-1.89	hydroxylation or epoxidation	5.60	-/-	+/+
M3	$C_{42}H_{60}NO_9^+$	+29.97418	722.42626	722.42655	0.39	demethylation to carboxylic acid or hydroxylation and ketone formation	5.57	-/-	+/+
M4	$C_{42}H_{62}NO_9^+$	+31.98983	724.44191	724.43915	-3.81	dihydroxylation	5.29	+/-	-/-
M5	$C_{42}H_{64}NO_9^+$	+34.00548	726.45756	726.45599	-2.16	alkene to dihydrodiol	5.28	-/+	-/-

3.2 Activity of 13-SPX-C metabolites towards nicotinic acetylcholine receptors

To determine if the metabolism of 13-SPX-C by S9 liver fractions leads to a decrease of toxicity mediated by acetylcholine receptor inhibition, the affinity of the S9-incubated samples, containing mostly 13-SPX-C metabolites, was tested with the *Torpedo*-nAChR-binding assay. Samples from rat S9 fraction decreased the competitive binding of biotin α-BgTx to the receptor by ~39%, as compared to non-metabolized 13-SPX-C (Table 2). In the case of human S9 fraction, an average decrease of ~21% of the inhibition was observed compared to control (Table 2).

Table 2. Functional activity of S9 incubation samples. Following 13-SPX-C incubation with rat and human S9 fraction, the antagonistic activity of the samples was tested against *Torpedo*-nAChRs using a non-radioactive microplate receptor-binding assay. Data represent the mean ± SD of two independent experiments performed in triplicates.

Treatment	**13-SPX-C** Inhibition (%)	**S9 incubation samples** Inhibition (%)	**Δ inhibition (%)**
Rat S9 Phase I + II (exp #1)	54.4 ± 5.5	15.5 ± 1.7	38.9
Human S9 Phase I + II (exp #1)	52.7 ± 5.4	33.2 ± 1.0	19.5
Human S9 Phase I + II (exp #2)	58.7 ± 6.1	37.0 ± 2.1	21.7

3.3 Effects of 13-SPX-C on the expression of nuclear receptors and drug-metabolizing enzymes in HepaRG cells

Gene expression levels in human HepaRG liver cells were analyzed by qRT-PCR after 24 h treatment with 33 and 66 nM 13-SPX-C, two concentrations which were not cytotoxic (Ferron et al., 2016). Expression of a selection of genes encoding drug-metabolizing phase I and II enzymes as well as uptake and efflux transporters and nuclear receptors involved in the regulation of drug metabolism was analyzed. While no effect regarding nuclear receptors was observed, the phase I gene *CYP1A2* was strongly up-regulated at 66 nM 13-SPX-C (5.8 fold), whereas the other CYPs were not remarkably affected (Table 3). The results on phase II genes showed a slight up-regulation of *NAT1* (1.7 fold) at 33 nM 13-SPX-C. Regarding uptake transporters, an up-regulation of *SLC22A3* (1.9 fold) was observed at 66 nM 13-SPX-C. No particular effects on efflux transporters were noticed. Omeprazole (50 µM) and rifampicin (10 µM) used as positive controls clearly showed an up-regulation for several *CYP* genes. Considering the up-regulation of *CYP1A2* gene expression by 13-SPX-C, we investigated if this enzyme could be involved in the metabolism of 13-SPX-C using CYP1A2-Silensomes™ tool.

Table 3. Effects of 13-SPX-C on mRNA expression in HepaRG cells. Cells were treated with two concentrations of 13-SPX-C for 24 h. Rifampicin (10 µM) and omeprazole (50 µM) were used as positive controls. Results were obtained from three independent experiments. Data represents means ± SD of fold change compared to solvent control. *$p < 0.05$, **$p < 0.01$, ***$p < 0.001$ after one-way ANOVA followed by Dunnett's post hoc tests.

Metabolism Phases	Gene	[nM]				OME		RIF	
		33		66					
		Mean	SD	Mean	SD	Mean	SD	Mean	SD
Nuclear receptors	*AHR*	1.2	0.4	1.0	0.5	0.7	0.1	0.9	0.4
	NR1I2	1.6	0.3	1.5	0.4	0.3	0.6	0.9	0.4
Phase 0 influx transporters	*SLC22A1*	1.2	0.2	1.2	0.1	0.9	0.2	1.0	0.4
	SLC22A3	1.4	0.3	1.9*	0.1	0.9	0.4	1.1	0.5
	SLCO1A2	0.7	0.4	0.6	0.7	0.4	0.5	0.2	0.2
	SLCO1B1	1.1	0.5	0.8	0.2	0.6	0.2	1.1	0.6
Phase I mono-oxygenases	*CYP1A1*	1.9	1.2	1.4	1.5	122.9***	55.5	0.4	0.4
	CYP1A2	1.7	0.3	5.8***	0.6	199.0**	119.4	1.4	0.9
	CYP2B6	1.2	0.2	1.5	0.3	4.7**	1.4	3.2*	1.2
	CYP2C9	1.1	0.1	1.1	0.3	1.3	0.5	2.1*	0.7
	CYP2C19	1.1	0.1	1.3	0.4	1.1	0.2	1.6	0.8
	CYP3A4	1.0	0.1	1.0	0.4	12.9	4.8	29.7***	11.1
	CYP3A5	1.0	0.2	1.0	0.3	1.0	0.2	1.5	0.4
Phase II transferases	*GSTM1*	1.0	0.3	1.3	0.2	1.2	0.2	1.1	0.4
	NAT1	1.7*	0.4	1.3	0.2	1.0	0.2	1.0	0.3
	NAT2	1.1	0.3	1.0	0.1	0.8	0.2	0.8	0.3
	SULT1A1	1.0	0.0	0.9	0.2	0.9	0.1	1.0	0.1
	SULT1E1	0.9	0.1	0.7	0.5	0.4	0.1	0.6	0.1
	UGT1A1	1.4	0.2	1.5	0.8	2.3*	0.0	1.7	0.6
	UGT1A9	1.1	0.0	1.0	0.3	1.2	0.3	1.2	0.5
	UGT2B4	1.2	0.2	1.1	0.3	1.3	0.2	1.4	0.4
Phase III efflux transporters	*ABCB1*	1.2	0.1	1.3	0.1	1.3	0.1	1.7	0.6
	ABCC2	1.3	0.1	1.3	0.2	1.2	0.2	1.2	0.4
	ABCC3	1.0	0.1	1.3	0.2	1.0	0.1	0.9	0.3
	ABCG2	1.2	0.1	1.0	0.4	2.3**	0.5	1.1	0.5

0.4 0.8 1.6 3 5

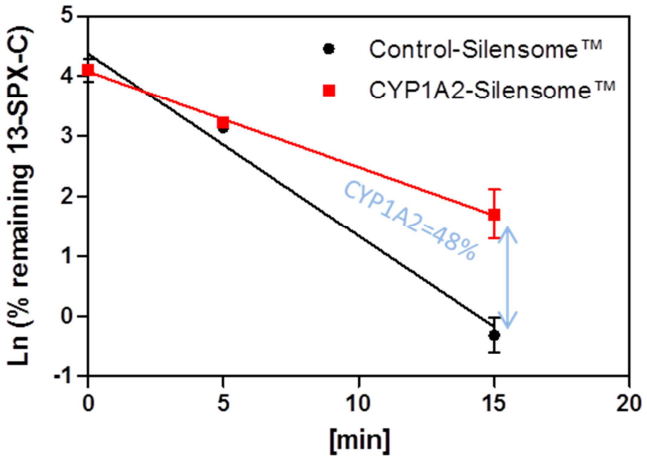
x-Fold change compared to solvent control

3.5 13-SPX-C phase I metabolism using CYP1A2-Silensomes™

As the induction of CYP1A2 expression in 13-SPX-C-treated HepaRG cells may be indicative of a role of this enzyme in 13-SPX-C metabolism, CYP1A2- Silensomes™ were incubated with 100 nM 13-SPX-C. The depletion of 13-SPX-C over time is shown in Figure 2. When 13-SPX-C was incubated with control-Silensomes™ the toxin was not detected anymore after 15 min. A slower depletion was observed when CYP1A2 was inhibited. From the depletion curves, we estimated that the *in vitro* intrinsic clearance (Cl_{int}) was

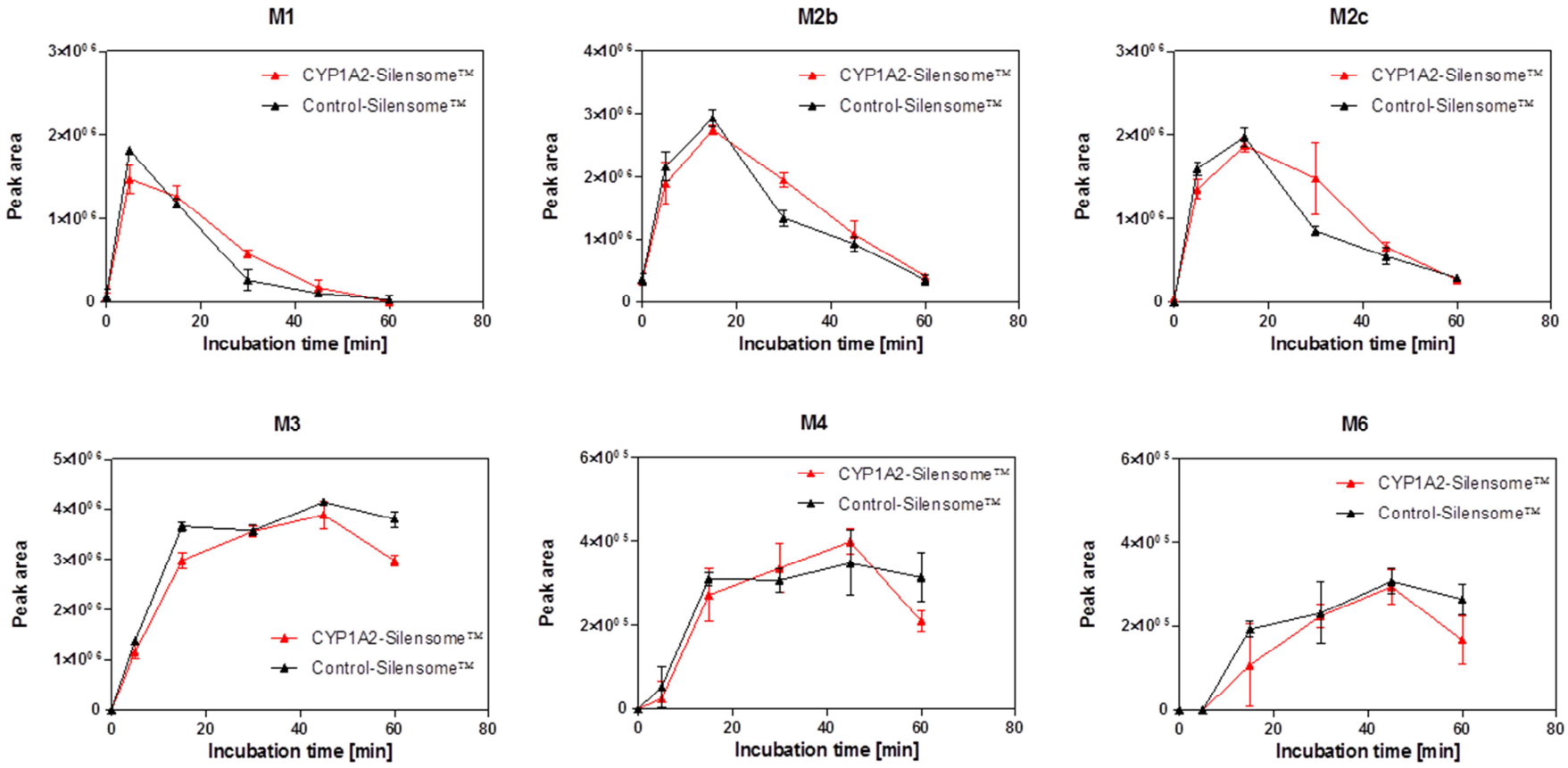
approximately bisected with CYP1A2-Silensomes™ (159.1 ± 12.2 µL×min^{-1}×mg^{-1}), as compared to controls (303.4 ± 21.5 µL×min^{-1}×mg^{-1}). From these data, the CYP1A2 *fm* was evaluated to be 48%.

Figure 2. 13-SPX-C kinetics with CYP1A2-Silensomes™. 100 nM 13-SPX-C was incubated with co-factors and microsomes for different times. Results were obtained from three independent experiments (each performed in triplicate determinations) and conducted with the same Silensomes™ batch. Data represents means ± SD.



The occurrence of metabolites from the experiments with the Silensomes™ was also investigated as described above. For both, homologous control Silensomes™ and CYP1A2-Silensomes™ six different metabolites were found, including a previously not detected metabolite featuring *m/z* 710.42626 (M6) (Figure 3). M1, M2b and M2c were detected but disappeared with time, whereas M3 was stable. For each metabolite, no difference of peak area was observed between homologous control Silensomes™ and CYP1A2-Silensomes™, indicating that the identified metabolites were not produced by CYP1A2.

Figure 3. Metabolite kinetics during incubation with CYP1A2-Silensomes™ and respective controls. Results were obtained from three independent experiments performed in triplicates. Data represents means ± SD.



4. Discussion

In this study, we assessed the metabolism of 13-SPX-C with rat and human liver S9 fractions, the toxicity of the incubation samples containing mostly 13-SPX-C metabolites as well as a preliminary investigation on the metabolic pathways involved.

Using human liver S9 fractions, we observed a full depletion of 13-SPX-C simultaneously to the formation of three phase I metabolites within 3 hours. All phase I metabolites featured same accurate masses as those who were described with HLM (Hui et al., 2012). Our inability to detect the other metabolites that were reported may be related to the lower concentration of toxin used in our experiments (100 nM compared to 10.2 µM used by Hui et al) or to the metabolic system (HLM displaying higher CYP content than S9 fraction). Using rat S9 fractions, a similar depletion of 13-SPX-C was observed simultaneously to the formation of four phase I metabolites featuring accurate masses that were also described with HLM (Hui et al., 2012). Only one metabolite with the same accurate mass (*m/z* 708.44699) was detected in both rat and human samples but different retention times were found between rat and human. This may indicate that the biotransformation occurred on a different site of the 13-SPX-C toxin, meaning that the metabolites could be isomers. As isomers can display great differences in pharmacokinetics and pharmacodynamics (Chhabra et al., 2013), if it turns out that some metabolites from rat S9 fraction are isomers of those produced with human S9 fraction, additional studies will be required to elucidate their toxic potential. No phase II metabolites were detected despite the formation of mono-oxygenated metabolites. Nevertheless, we cannot conclude that phase II processes do not play a role in the biotransformation of 13-SPX-C as all phase II reactions were not investigated (e.g. acetylation or methylation).

We demonstrated that 13-SPX-C was completely biotransformed into several metabolites by rat and human liver S9 fractions. Then, we assessed how metabolism can affect the toxicity by studying the capacity of the incubation samples to inhibit muscle nicotinic acetylcholine

receptors in comparison with the parent compound (Aráoz et al., 2015). If metabolite-containing samples produced by both rat and human liver S9 fractions showed a decreased affinity for nicotinic acetylcholine receptors, human samples were nonetheless twice as much potent than those from rat samples, possibly indicating that one human metabolite may retain an affinity for nicotinic acetylcholine receptors. As no individual standard for the metabolites is currently available, it is not possible to assess neither their own biological activity nor quantifying their amount in the incubation samples. Further studies should be addressed to assess the activity of each single metabolite on nAChR as well as on other cellular targets. A biogram analysis may be a suitable approach for such purpose (Leet et al., 2015). Considering that rat and human liver S9 fractions featured a different pattern of metabolites with different affinity for nicotinic acetylcholine receptors, rat may not be the most appropriate animal model to reflect the behavior of 13-SPX-C in humans.

We confirmed that 13-SPX-C undergoes an extensive biotransformation process by liver enzymes and, to get a closer look on the pathways involved, we investigated the modulation of a panel of metabolism-associated genes expression in human HepaRG cells by 13-SPX-C. We observed that 13-SPX-C particularly up-regulated *CYP1A2*. In human liver, CYP1A2 plays an important role in xenobiotic metabolism (about 10-20% of drugs are substrates of CYP1A2) (Omiecinski et al., 2011). Besides detoxification, CYP1A2 is also known to bioactivate some xenobiotics such as 1-nitropyrene or aflatoxin B1 (Yamazaki et al., 2000, Van Vleet et al., 2002). To point out if this enzyme was implied in 13-SPX-C metabolism, we used the innovative Silensomes™ tool. We found that the contribution of CYP1A2 was estimated to 48% in the biotransformation of 13-SPX-C, meaning that other(s) xenobiotic-metabolizing enzyme(s) (XME) likely participate in 13-SPX-C metabolism. Six phase I metabolites featuring accurate masses that were described by Hui et al., 2012 were detected in this study but no differences in the metabolites´ peak areas between control and CYP1A2-

Silensomes™ were observed. This suggests that metabolites were likely produced by a different CYP as the presence or absence of CYP1A2 did not modify their formation. A possible explanation is that CYP1A2 catalysed the formation of reactive metabolites with too short half-lifes to be detected within our experimental conditions.

Since CYP1A2 is involved in 13-SPX-C biotransformation and that the toxin induced *CYP1A2*gene expression, it can be assumed that 13-SPX-C is an inducer of its own metabolism. Such phenomenon has already been described for several compounds (Berthou et al., 1998, Aimova et al., 2007).

The high rate of 13-SPX-C metabolism coupled to the formation of less potent metabolites towards nAChR may explain why a low oral dose of 13-SPX-C was not toxic to mice (Otero et al. 2012) and why no acute human intoxications related to 13-SPX-C shellfish contamination have been reported to date.

5. Conclusions

In conclusion, we showed that 13-SPX-C undergoes extensive phase I metabolism using liver S9 fractions leading to the formation of several oxidized metabolites. We clearly showed that CYP1A2 was involved in the biotransformation of this toxin, but other XMEs are also expected to be implied. The metabolites formed were less potent towards the nicotinic acetylcholine receptor assay compared to the parent compound, indicating that hepatic metabolism participates in the detoxification of 13-SPX-C.

Conflict of interest

The authors declare no conflict of interest in the content of this work.

Acknowledgments

We would like to thank Jean-Michel Delmas from the ARC unit for his excellent support and advices on Orbitrap. We would like to thank Patrick Fach and Cédric Woudstra from the IdentyPath platform (Anses Maisons-Alfort) for their excellent support and advices on qRT-PCR assays. We would like to thank Abdelhafidh Belakermi from Bioprédic International for his help on Silensomes™ assays. We would like to thank Uta Herfurth from the BfR for her proof-reading of the manuscript.

Funding information

This work was financed by the French Agency for Food, Environmental and Occupational Health & Safety (ANSES) and by the German Federal Institute for Risk Assessment (BfR).

References

Aimova, D.; Svobodova, L.; Kotrbova, V.; Mrazova, B.; Hodek, P.; Hudecek, J.; Václavíková, R.; Frei, E.; Stiborová, M. The Anticancer Drug Ellipticine Is a Potent Inducer of Rat Cytochromes P450 1A1 and 1A2, Thereby Modulating Its Own Metabolism. Drug Metab. Dispos. 2007, **35**, 1926–1934.

Amzil Z, Sibat M, Royer F, Masson N, Abadie E. (2007). Report on the first detection of pectenotoxin-2, spirolide-A and their derivatives in French shellfish. *Mar Drugs*. **5(4),** 168–179.

Aráoz, R., Ramos, S., Pelissier, F., Guérineau, V., Benoit, E., Vilariño, N., Botana, L.M., Zakarian, A. and Molgó, J. (2012). Coupling the *Torpedo* microplate-receptor binding assay with mass spectrometry to detect cyclic imine neurotoxins. *Anal Chem*. **84(23),** 10445-10453.

Aráoz R, Ouanounou G, Iorga BI, Goudet A, Alili D, Amar M, et al. (2015). The Neurotoxic Effect of 13,19-Didesmethyl and 13-Desmethyl Spirolide C Phycotoxins Is Mainly Mediated by Nicotinic Rather Than Muscarinic Acetylcholine Receptors. *Toxicol Sci*. **147(1),** 156–67.

Berthou, F.; Goasduff, T.; Dreano, Y.; Ménez, J.-F. Caffeine increases its own metabolism through cytochrome P4501A induction in rats. Life Sci. 1998, **57**, 541–549.

Bourne, Y., Radic, Z., Aráoz, R., Talley, T. T., Benoit, E., Servent, D., Taylor, P., Molgó, J., and Marchot, P. (2010). Structural determinants in phycotoxins and AChBP conferring high affinity binding and nicotinic AChR antagonism. Proc. Natl. Acad. Sci. USA **107**, 6076–6081.

Cembella, A.D., Lewis, N.I., Quilliam, M.A., (2000). The marine dinoflagellate Alexandriumostenfeldii (Dinophyceae) as the causative organism of spirolide shellfish toxins. *Phycologia* **39,** 67–74.

Chhabra N, Aseri ML, Padmanabhan D. (2013). A review of drug isomerism and its significance. *Int J Appl Basic Med Res*. **3,**16–18.

EFSA Panel on Contaminants in the Food Chain (CONTAM); Scientific Opinion on marine biotoxins in shellfish – Cyclic imines (spirolides, gymnodimines, pinnatoxins and pteriatoxins). EFSA Journal 2010; 8(6):1628. [39 pp.]. doi:10.2903/j.efsa.2010.1628. Available online: www.efsa.europa.eu

Espiña B, Otero P, Louzao MC, Alfonso A, Botana LM. (2011). 13-Desmethyl spirolide-c and 13,19-didesmethyl spirolide-c trans-epithelial permeabilities: Human intestinal permeability modelling. *Toxicology* **287(1–3),** 69–75.

Gill S, Murphy M, Clausen J, Richard D, Quilliam M, MacKinnon S, et al. (2003). Neural Injury Biomarkers of Novel Shellfish Toxins, Spirolides: A Pilot Study Using Immunochemical and Transcriptional Analysis. *NeuroToxicology* **24(4–5),** 593–604.

Hill J.A., Jr., Nghiem H.O., Changeux J.P. Serine-specific phosphorylation of nicotinic receptor associated 43 K protein. Biochemistry. 1991;**30**:5579–5585.

Hui JPM, Stuart Grossert J, Cutler MJ, Melanson JE. (2012). Strategic identification of *in vitro* metabolites of 13-desmethyl spirolide C using liquid chromatography/high-resolution mass spectrometry: Identification of *in vitro* metabolites of 13-desmethyl spirolide C. *Rapid Commun Mass Spectrom.* **26(3),** 345–54.

Le Hegarat, L., Dumont, J., Josse, R., Huet, S., Lanceleur, R., Mourot, A., Poul, J.-M., Guguen-Guillouzo, C., Guillouzo, A., and Fessard, V. (2010). Assessment of the genotoxic potential of indirect chemical mutagens in HepaRG cells by the comet and the cytokinesis-block micronucleus assays. *Mutagenesis* **25,** 555–560.

Leet JE, Belcastro JV, Dowling CJ, et al. HPLC biogram analysis: a powerful tool used for hit confirmation in early drug discovery. J Biomol Screen. 2015;**20(5)**:681–687.

Miles CO, Rundberget T, Sandvik M, Aasen JAB and Selwood AI, 2010. The presence of pinnatoxins in Norwegian mussels. Report 07b - 2010, Veterinærinstituttet, National Veterinary Institute. Available from http://www.vetinst.no/eng/Research/Publications/Report-Series/Rapportserie-2010/7b-2010-The-presence-of-pinnatoxins-in-Norwegian-mussels.

Munday R, Quilliam MA, LeBlanc P, Lewis N, Gallant P, Sperker SA, Ewart HS, MacKinnon SL. (2012). Investigations into the toxicology of spirolides, a group of marine phycotoxins. *Toxins.* **4(1),** 1-14.

Omiecinski CJ, Vanden Heuvel JP, Perdew GH, Peters JM. (2011). Xenobiotic Metabolism, Disposition, and Regulation by Receptors: From Biochemical Phenomenon to Predictors of Major Toxicities. *Toxicol Sci*. **120(Supplement 1),** S49–75.

Otero P, Alfonso A, Rodríguez P, Rubiolo JA, Cifuentes JM, Bermúdez R, et al. (2012). Pharmacokinetic and toxicological data of spirolides after oral and intraperitoneal administration. *Food Chem Toxicol*. **50(2),** 232–7.

Parmentier Y, Pothier C, Delmas A, et al. (2017). Direct and quantitative evaluation of the human CYP3A4 contribution (fm) to drug clearance using the in vitro SILENSOMES model. Xenobiotica Fate Foreign Compd Biol Syst **47**:562–75.

Picot C, Limon G, Durand G, Parent-Massin D, Roudot AC. (2013). Probabilistic dietary exposure to phycotoxins in a recreational shellfish harvester subpopulation (France). *J Expo Sci Environ Epidemiol*. **23(4),** 435-441.

Rubio, F., Kamp, L., Carpino, J., Faltin, E., Loftin, K., Molgó, J. and Aráoz, R. (2014). Colorimetric microtiter plate receptor-binding assay for the detection of freshwater and marine neurotoxins targeting the nicotinic acetylcholine receptors. *Toxicon* **91,** 45-56

Touzet, N., Franco, J.M., Raine, R., (2008). Morphogenetic diversity and biotoxin composition of Alexandrium (dinophyceae) in Irish coastal waters. *Harmful Algae* **7,** 782-797.

Van Vleet TR, Mace K, Coulombe Jr RA. (2002). Comparative Aflatoxin B1 Activation and Cytotoxicity in Human Bronchial Cells Expressing Human CYPs 1A2 and 3A4. *ADVS Fac Publ*.**16.**

Vilariño, N., Fonfría, E.S., Aráoz, R., Molgó, J. and Botana, L.M. (2009). Detection of gymnodimine-A and 13-desmethyl C spirolide phycotoxins by fluorescence polarization. *Anal Chem*. **81,** 2708-2714.

Yamazaki H, Hatanaka N, Kizu R, Hayakawa K, Shimada N, Guengerich FP, et al. (2000). Bioactivation of diesel exhaust particle extracts and their major nitrated polycyclic aromatic hydrocarbon components, 1-nitropyrene and dinitropyrenes, by human cytochromes P450 1A1, 1A2, and 1B1. *Mutat Res Toxicol Environ Mutagen*. **472(1),** 129–138.

National Center for Biotechnology Information (NCBI). GenBank Sequence Database. Available online: http://www.ncbi.nlm.nih.gov/ (accessed on 11 January 2017).

National Center for Biotechnology Information (NCBI). Primer Designing Tool. Available online: http://www.ncbi.nlm.nih.gov/tools/primer-blast/index.cgi?LINK_LOC=BlastHome (accessed on 15 January 2017).

Appendices

Table A.1 Summary of primers used for q-PCR analysis.

Gene	Sequence (5' to 3')	Gene	Sequence (5' to 3')
AHR	F: TAGGGTTTCAGCAGTCTGATGTC R: CTACTGTCTGGGGGAGACCA	*SULT1E1*	F: ACAGGATCAACTAAACAGTGTACCA R: ATCTGGTCTTGCCTGGAACG
NR1I2	F: AGACACTGCAGGTGGCTTC R: TGGGGAGAAGAGGGAGATGG	*UGT1A1*	F: CTGCCTTCACCAAAATCCACTATC R: CACAGGACTGTCTGAGGGATTT
CYP1A1	F: ACCCTGAAGGTGACAGTTCC R: TCTTGGAGGTGGCTGAGGTA	*UGT1A9*	F: CGGAGTATGATCTCTACAGCCAC R: TTCAAATTCCATAGGCAACGGC
CYP1A2	F: CTTCGCTACCTGCCTAACCC R: CCCGGACACTGTTCTTGTCA	*UGT2B4*	F: GAAGTTCTAGGAAGACCCACTACG R: GGGTGAGGAAATTGAAAATCCCAG
CYP2B6	F: TTCGGCGATTCTCTGTGACC R: ATGAGGGCCCCCTTGGAT	*ABCB1*	F: CAGCTGTTGTCTTTGGTGCC R: CCAATGTGTTCGGCATTAGGC
CYP2C9	F: AAATGGAGAAGGAAAAGCACAACC R: TCAACTGCAGTGTTTTCCAAGC	*ABCC2*	F: GTGTGGATTCCCTTGGGCTT R: GAAGAAAACCAACGAATACCTGCTT
CYP2C19	F: CCTGGAACGCATGGTGGT R: TCCATTGCTGAAAACGATTCCAAAT	*ABCC3*	F: CCAACTCAGTCAAACGTGCG R: ACCTAGGTTCTGCCAGAGGA
CYP3A4	F: TCACAAACCGGAGGCCTTTT R: TGGTGAAGGTTGGAGACAGC	*ABCG2*	F: AGTTCTCAGCAGCTCTTCGG R: TTCCAACCTTGGAGTCTGCC
CYP3A5	F: GCCCAATAAGGCACCACCTA R: CCACCATTGACCCTTTGGGA	*SLC22A1*	F: TGTCAAATTTGTTGGCGGGG R: TTTAACCAGTGCAGGTCAGGT
GSTM1	F: GGGGGACGCTCCTGATTATG R: GGGCAGATTGGGAAAGTCCA	*SLC22A3*	F: GCATTGCTAAGTGCAATGGGA R: GCTTGTGAACCAAGCAAACATAAG
NAT1	F: ACTAAGAAAGGGGATCATGGACATT R: ACAGCTCGGATCTGGTGTTG	*SLCO1A2*	F: GCACAAGAGTATTTGCTGGCAT R: CGGCAATCCGAGGTAGATGT
NAT2	F: ACAGACCTTGGAAGCAAGAGG R: CTTCAATGTCCATGATCCCTTTGG	*SLCO1B1*	F: TCCACATCATTTTCAAGGGTCTACT R: TGCTTCATCCATGACACTTCCAT
SULT1A1	F: TCGGAGAAGTGTCCTACGGAT R: CCACGAAGTCCACGGTCTC	*GAPDH*	F: GTCAAGGCTGAGAACGGGAA R: AAATGAGCCCCAGCCTTCTC

Table A.2 Reactions screened using MetWorks® 1.3.

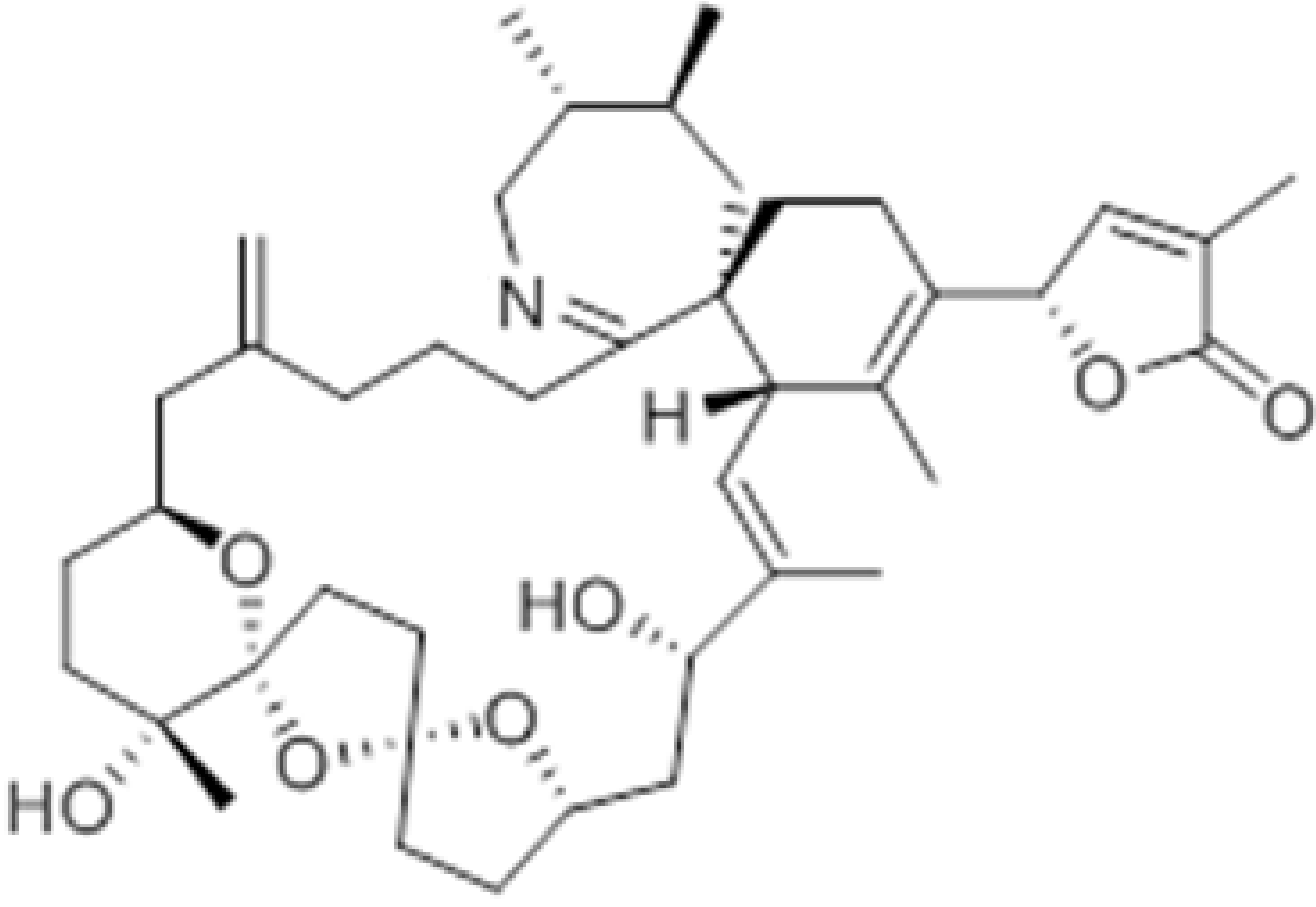
Reaction	Mass shift	Reaction	Mass shift
Acetylation	+42.01056	Hydroxylation and desaturation	+13.97926
N-acetylcysteine conjugation	+161.01466	Hydroxylation and ketone formation	+29.97418
Alcohols dehydration	-18.01056	Hydroxymethylene loss	-30.01056
Alkenes to dihydrodiol	+34.00548	Hydroxylation and Methylation	+30.01056
Aromatic thiols to sulfonic acids	+47.98474	Hydroxylation and Ethylation	+45.03404
Cysteine conjugation	+103.00918	Isopropyl dealkylation	-42.04695
S-cysteine conjugation	+119.00410	Isopropyl to acid	-14.05204
Debenzylation	-90.04695	Isopropyl to alcohol	-26.05204
Decarboxylation	-43.98983	Nitro-reduction	-29.97418
Decarbonylation	-27.99491	Methylation (O, N, S)	+14.01565
Deethylation (N,S,O)	-28.03130	Methyl ketone to acid	-12.03639
Demethylation (N,S,O)	-14.01565	Methylene to ketone	+13.97926
Demethylation and hydroxylation	+1.97926	Oxidation +O	+15.99491
Demethylation and two hydroxylations	+17.97418	Oxidative Deamination	-1.03163
Demethylation and methylene to ketone	-0.03639	Oxidative debromination	-63.93125
Demethylation to carboxylic acid	+29.97418	Oxidative dechlorination	-19.98176
Desaturation	-2.01565	Oxidation-Demethylation	+1.97926
Desaturations x2	-4.03130	Oxidation-De-ethylation	-12.03639
2-ethoxyl to acid	-0.03639	Propyl ether to acid	-28.06769
Ethyl ether to acid	-14.05204	Propyl ketone to acid	-40.06769
Ethyl ketone to acid	-26.05204	Quinone formation	+29.97418
Ethyl to alcohol	-12.03639	Reduction	+2.01565
Ethyl to carboxylic acid	+15.95853	Sulfation	+79.95681
Glucuronidation (O, N, S)	+176.03209	Disulfation	+159.91363
Glucuronidation (O, N, S) and Hydroxylation	+192.02700	Sulfation and Hydroxylation	+95.95173
Glucuronidation and Decarboxylation	+148.03717	Sulfoxide to thioether	-15.99491
Glucuronidation + De-ethlylation (O, N, S)	+148.00079	Taurine conjugation	+107.00410
Glucuronidation + De-methylation (O, N, S)	+162.01644	Thioether to sulfone	+31.98983
Glutathione conjugation	+307.08381	Thioureas to ureas	-15.97716
S-GSH conjugation and Epoxidation	+323.07872	Trifluoromethyl loss	-67.98738
S-GSH conjugation and Desaturation	+305.06816	*Tert*-butyl to acid	-28.06769
Glycine Conjugation (Carboxylic acids)	+57.02146	*Tert*-butyl to alcohol	-40.06769
Hydrolysis	+18.01056	*Tert*-butyl dealkylation	-28.03130
Hydrolysis of nitrate esters	-44.98508		

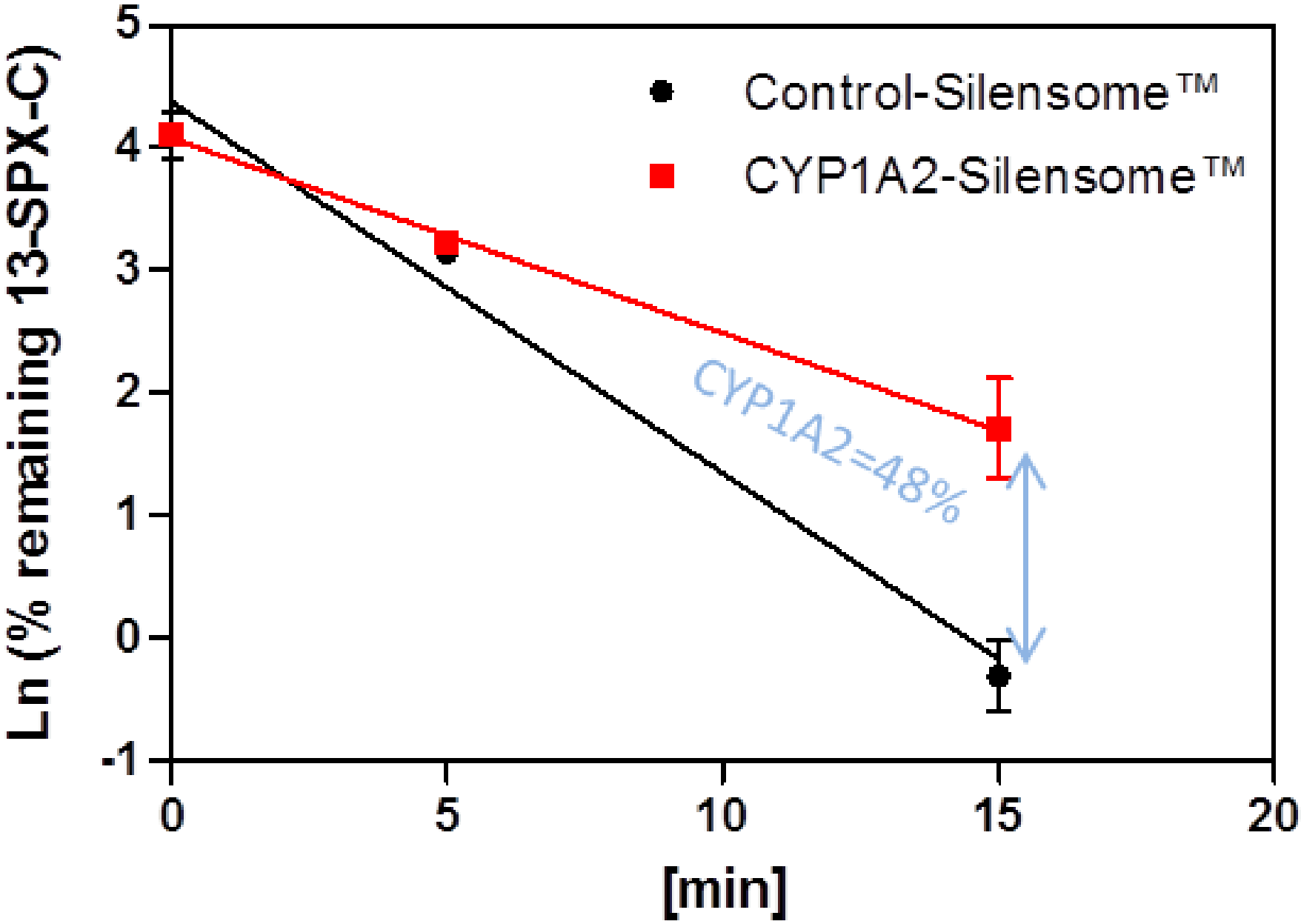
Table A.3 13-SPX-C recovery after incubation with rat and human inactivated S9 fractions. S9 fractions were heat-inactivated for 45 min before a 3 hour-incubation with specific phase I and II co-factors and 100 nM 13-SPX-C. Results were obtained from two independent experiments conducted with the same S9 batches.

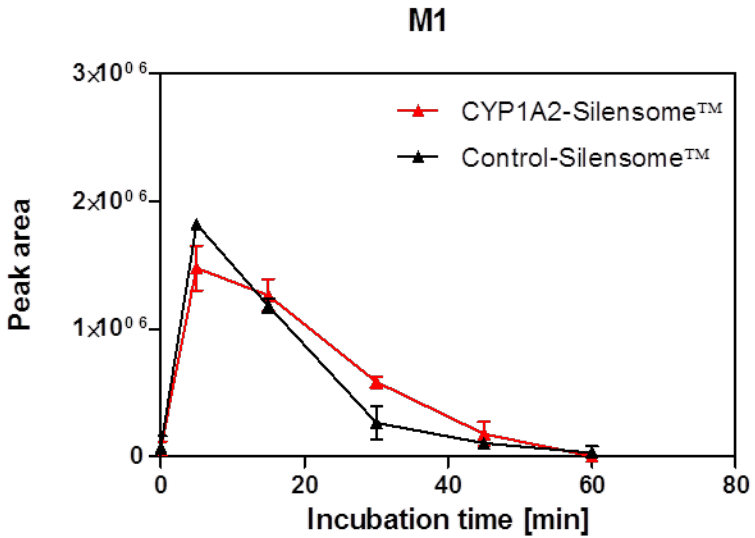
Assay	Inactivated Rat S9	Inactivated Human S9
#1	71 ± 3%	86 ± 2%
#2	105 ± 5%	88 ± 1%

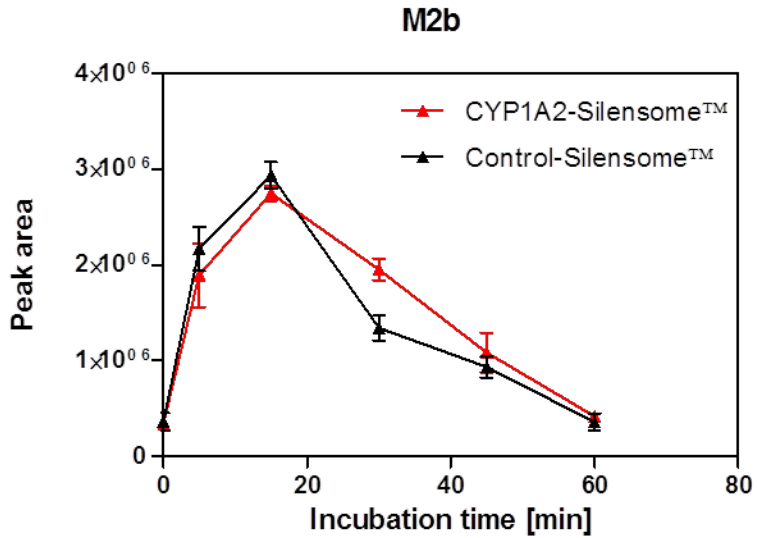
Table A.4 13-SPX-C depletion after incubation with rat and human S9 fractions. S9 fractions were incubated for 3 h with specific phase I and II co-factors and 100 nM 13-SPX-C. Results were obtained from two independent experiments conducted with the same S9 batches.

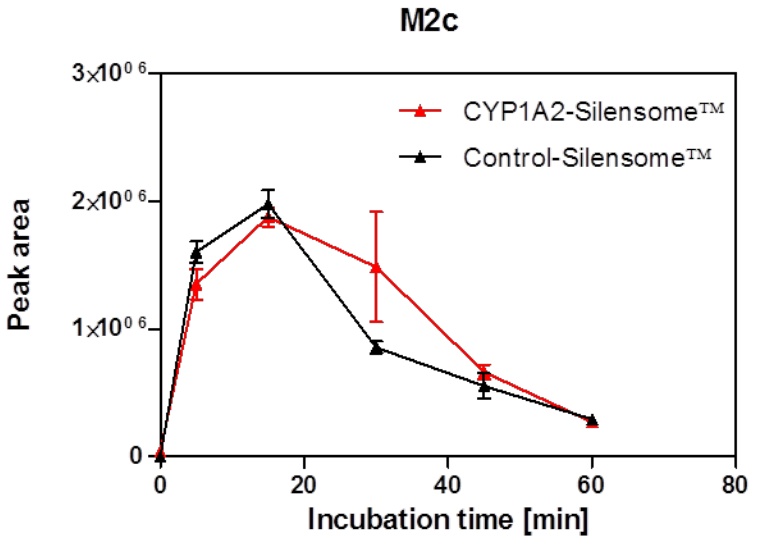
Assay	Native Rat S9	Native Human S9
#1	100 ± 0%	100 ± 0%
#2	93 ± 1%	100 ± 0%

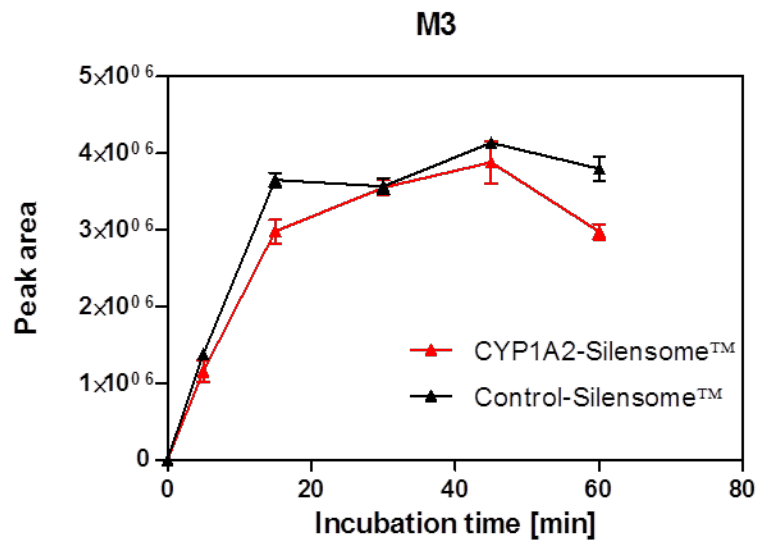

N
H
O
O
HO
O
O
O
HO

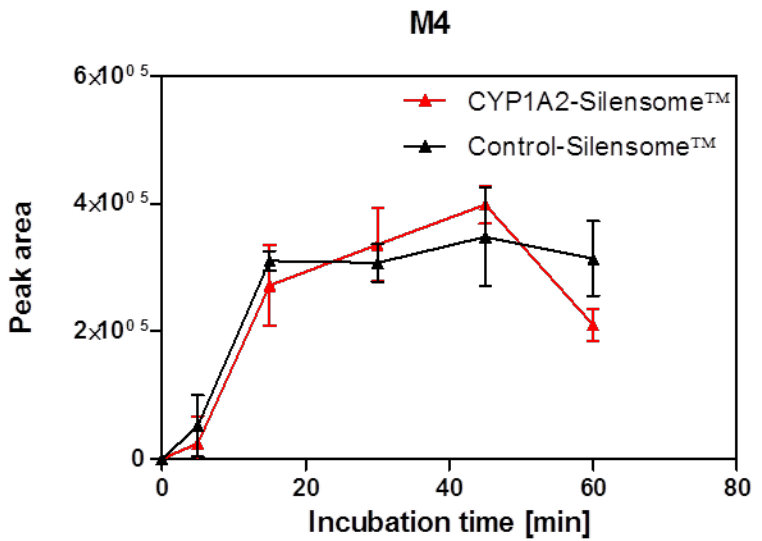

Control-Silensome™
CYP1A2-Silensome™
CYP1A2=48%
Ln (% remaining 13-SPX-C)
[min]
5
4
3
2
1
0
-1
0
5
10
15
20

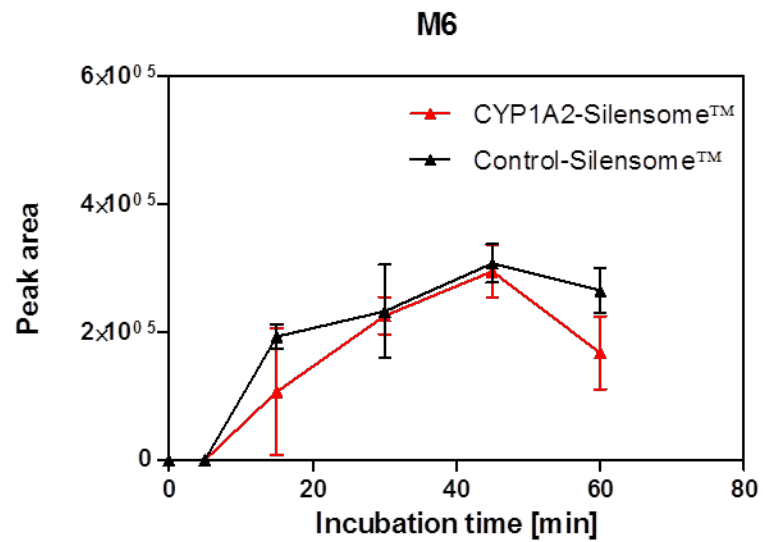

M1
Peak area
3x10^6
2x10^6
1x10^6
0
0
20
40
60
80
Incubation time [min]
CYP1A2-Silensome™
Control-Silensome™


M2b
Peak area
4x10^6
3x10^6
2x10^6
1x10^6
0
0
20
40
60
80
Incubation time [min]
CYP1A2-Silensome™
Control-Silensome™


M2c
Peak area
3x10^6
2x10^6
1x10^6
0
0
20
40
60
80
Incubation time [min]
CYP1A2-Silensome™
Control-Silensome™


M3
Peak area
5x10^6
4x10^6
3x10^6
2x10^6
1x10^6
0
0
20
40
60
80
Incubation time [min]
CYP1A2-Silensome™
Control-Silensome™


M4
Peak area
6x10^5
4x10^5
2x10^5
0
0
20
40
60
80
Incubation time [min]
CYP1A2-Silensome™
Control-Silensome™


M6
Peak area
6x10^5
4x10^5
2x10^5
0
0
20
40
60
80
Incubation time [min]
CYP1A2-Silensome™
Control-Silensome™